RSC Advances

PAPER

View Article Online
View Journal | View Issue

Cite this: *RSC Adv.*, 2026, **16**, 18330

Push–pull benzophenone derivative-based visible photoinitiating systems: synthesis, characterization, properties, and application for free radical photopolymerization under LEDs

Qingqing Wu, *[a] Jingdong Guo,[a] Mingsen Deng[b] and Fushao Li[a]

This study presents four (4-benzylamino-3-nitrophenyl) (phenyl)methanone derivatives (**BP-NBR**). They exhibit broad absorption peaks in the wavelength region of 350–500 nm, exhibiting a fairly good overlap with the emission spectra of light-emitting diodes (LEDs). In the presence diaryliodonium (Iod) or ethyl 4-(dimethylamino)benzoate (EDB), **BP-NBR** show high efficiency, although they show low activity as one-component system upon LED exposure. The proposed mechanism is as follows: the benzophenone segment is inactive due to its non-coplanar benzene groups. Instead, the 2-benzylamino-nitrophenyl segment serves as the photosensitizer. Moreover, the para-substituent of the benzylamino group has an effect on its initiation efficiency. The photoinitiation rate offered by **BP-NBR**/EDB is faster than that offered by the commercial photoinitiator 4-aminobenzophenone ($BPNMe_2$)/EDB system upon exposure to 450 nm LED light. Thus, **BP-NBR** exhibit application potential in long wavelength LED photopolymerization.

Received 7th February 2026
Accepted 20th March 2026

DOI: 10.1039/d6ra01087c

rsc.li/rsc-advances

1. Introduction

Photopolymerization has garnered significant attention over the past few decades as an alternative to traditional thermal polymerization. As it proceeds in the absence of solvents and offers excellent spatiotemporal control,[1–3] it has been adopted in a wide array of industrial applications. These range from their use in coatings and adhesives to electronic chips, dental resins, and advanced 3D/4D printing technologies.[4–12] The photoinitiator (PI) plays a pivotal role within a photocurable resin formulation.[13] It is responsible not only for initiating the photopolymerization reaction but also for determining the ultimate properties and performance of the cured materials.[14]

Recently, the development of photocurable resins that can be polymerized under visible light-emitting diode (LED) exposure has garnered considerable attention.[15–20] LED technology has developed rapidly in recent years and has gained widespread popularity due to its numerous advantages, including high-quality illumination, low energy consumption, the absence of ozone release, long operational lifetimes, and durability.[21] However, a critical challenge that remains to be solved is the mismatch between the absorption spectra of conventional photoinitiators (PIs) and the emission spectra of available light sources, such as in the case of UV-LEDs emitting above 365 nm and visible LEDs.[22] This mismatch results in inefficient excitation of PIs, which is often reflected in the low conversion of monomers to polymers. Consequently, the resulting material may contain unreacted and often toxic residual monomers. From an industrial perspective, this leads to significant economic losses due to increased raw material consumption, higher energy usage, and elevated production costs.[23,24] Therefore, there is an urgent need to develop novel PIs that are compatible with LED light sources, particularly those emitting at 405 nm or even 435 nm.

Simple diaryl iodonium salts are widely used as initiators for light-induced polymerization.[25–28] However, their absorption characteristics do not align with the emission spectra of commercially available light sources, including UV-A LEDs, visible LEDs, and even medium-pressure mercury lamps.[29] To address this limitation, it is necessary to develop high-performance initiation systems that combine an iodonium salt with a photosensitizer molecule capable of enhancing the polymerization initiation efficiency.[30–36] In this context, photosensitizers are required to enable the effective activation of iodonium salts under visible light irradiation.

As a UV PI, benzophenone is particularly useful; its versatility, low price, and strong absorption make it ideal for various applications. However, due to its maximum absorption wavelength of 257 nm, its absorption capacity in the visible light range is poor. With the development of LED light sources,

[a]*Guizhou Provincial Key Laboratory of Computational Nano-Material Science, Guizhou Education University, Guiyang, Guizhou, 550018, PR China. E-mail: 2011202030085@whu.edu.cn*

[b]*Laboratory for Solid-State Energy Storage and Intelligent System (SESIS-Lab), School of Information, Guizhou University of Finance and Economics, Guiyang, Guizhou 550025, PR China*

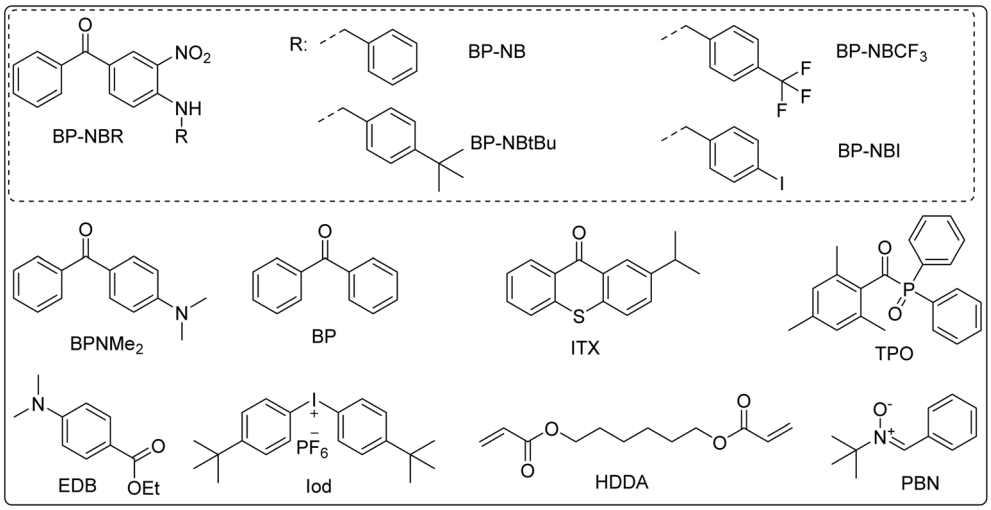

Scheme 1 Chemical structures of the PIs (**BP-NBR**, $BPNMe_2$, BP, ITX, and TPO), additives (EDB and Iod), monomer (HDDA), and capture agent (PBN).

broadening the absorption spectrum range of benzophenone series PIs has become an important research direction.[37–40] In the present work, (4-benzylamino-3-nitrophenyl)(phenyl) methanone derivatives were employed as photosensitizers in conjunction with iodonium salts, providing an efficient strategy for initiating and controlling photopolymerization processes. The presence of both amino (electron-donating) and nitro (electron-withdrawing) groups creates a push–pull system within the molecule, which facilitates an efficient intersystem crossing to the excited triplet state,[41,42] thereby enhancing the photosensitizing efficiency. Upon irradiation, these photosensitizers induce electron transfer to iodonium salts, generating reactive species that subsequently initiate the polymerization of monomers to polymers.

The structures of the investigated PIs, additives, monomer, and capture agent are shown in Scheme 1. Four new benzophenone derivatives (**BP-NBR**) with absorption at longer wavelengths than the commercial 4-(dimethylamino)benzophenone ($BPNMe_2$) were reported. These compounds were incorporated into two-component photoinitiating systems, namely, PI/Iod and PI/EDB, to generate active radicals for free radical polymerization upon visible light irradiation. The introduction of various substituents onto the benzophenone scaffold provided an opportunity to investigate the structure-reactivity-efficiency relationships of these derivatives as photosensitizers in free radical polymerization.

2. Results and discussion

2.1 Synthesis of BP-NBR

BP-NBR were synthesized by nucleophilic substitution between (4-amino-3-nitrophenyl)(phenyl)methanone and benzyl bromide derivatives. The synthetic route is shown in Scheme 2. The synthesis procedure and the ^1H NMR, ^{13}C NMR, FTIR, and HRMS spectra are shown in the SI.

2.2 Absorption properties of BP-NBR

The UV-visible absorption spectra of **BP-NBR** in acetonitrile are shown in Fig. 1a. The maximum absorption wavelengths (λ_{max}) were observed at 413 nm, 415 nm, 411 nm, and 409 nm for BP-NB, BP-NBtBu, BP-NBI, and $BP\text{-}NBCF_3$, respectively. Remarkably, **BP-NBR** exhibit a narrow absorption band in the near-UV region (350–450 nm), attributed to the $\pi \rightarrow \pi^*$ transitions. This spectral feature ensured a fairly good overlap with the emission spectra of the LEDs used in this work (at 405 nm, 435 nm and 450 nm). The maximum absorption wavelength of $BPNMe_2$ in acetonitrile located at 345 nm is considered for comparison.[43,44] **BP-NBR** display a redshift of approximately 65 nm in their λ_{max} relative to $BPNMe_2$, which is primarily ascribed to the enhanced intramolecular charge transfer (ICT) effect resulting from the presence of both nitro and benzylamino groups.[45] The theoretical absorption spectra of **BP-NBR** are presented in Fig. 1b–e. Based on the oscillator strength (f), the theoretical spectra reveal a weak excited singlet transition S_1 for all the variants. The calculated energy absorption bands are in agreement with the experimental data.

The optimized geometries and corresponding frontier molecular orbitals (highest occupied molecular orbital (HOMO) and lowest unoccupied molecular orbital (LUMO)) of **BP-NBR** were calculated using time-dependent density functional theory (TD-DFT) at the B3LYP/6-311g(d,p) level. Results are summarized in Table 1. The benzophenone segment in **BP-NBR** adopts a non-coplanar conformation, which may influence its photophysical behavior. The dihedral angles (θ) between the two

Scheme 2 Synthetic route of **BP-NBR**.

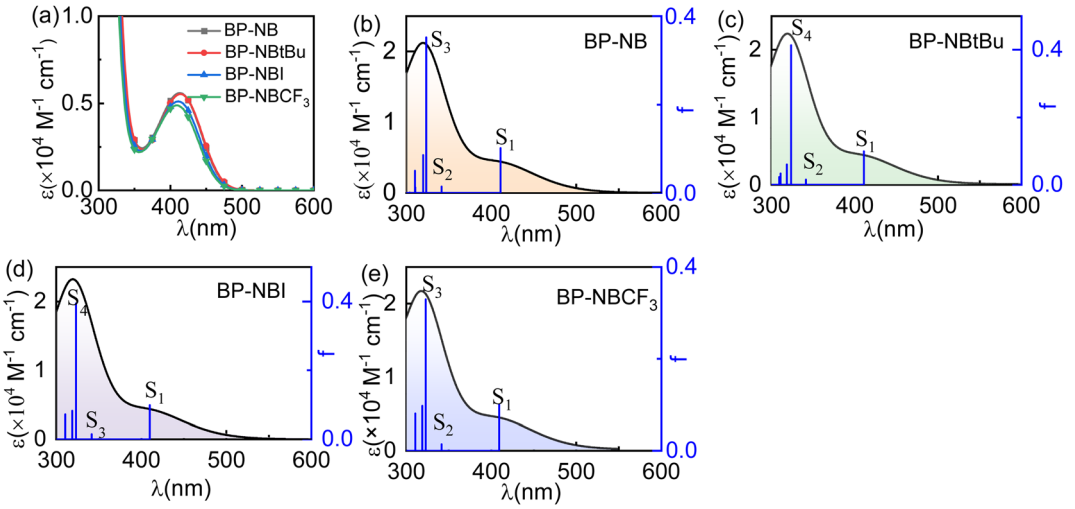

Fig. 1 (a) UV-vis absorption spectra of **BP-NBR** in acetonitrile ([**BP-NBR**] = 1.5 × 10^{-4} mol L^{-1}). (b)–(e) Theoretical UV-vis absorption spectra of **BP-NBR** in acetonitrile calculated using B3LYP/6-311g(d,p).

phenyl rings of the benzophenone segment are shown in Table 1, which were 50.5°, 50.6°, 50.6°, and 50.9° for BP-NB, BP-NBtBu, BP-NBI, and BP-$NBCF_3$, respectively. The large dihedral angles indicate a significant twist in the benzophenone core. The HOMO energy denotes the electron donation behavior of the molecular system, while the LUMO energy reflects its electron-accepting ability; these values govern the chemical stability of the molecule.[46]

The HOMO–LUMO energy gaps were calculated to be 3.54, 3.53, 3.54, and 3.55 eV for BP-NB, BP-NBtBu, BP-NBI, and BP-$NBCF_3$, respectively, indicating that the substituents had a negligible effect on the energy gap. Molecular orbital (MO) analysis revealed that all investigated compounds exhibited a charge transfer characteristic. For instance, in BP-NB, the HOMO was predominantly localized on the benzene ring, which is connected to the nitro group, whereas the LUMO was mainly localized on the nitro-benzene moiety. This spatial separation of the electron density upon excitation is a characteristic of ICT.

There was no fluorescence emission signal at an excitation wavelength of 420 nm. This is in accordance with the literature reports.[47–49] These reports indicate that a very short singlet lifetime and a rather large yield of phosphorescence are common features of such systems. However, the short lifetime of the triplet at room temperature did not allow its direct spectral characterization. The singlet excited states (S_1), the vertical excited state (S_v), and triplet states (T_1 and T_2) were calculated using TD-DFT, and their relative energies are depicted in Fig. 2 and Table S1. Upon photoexcitation, **BP-NBR** were

Table 1 Contour plots of the frontier molecular orbitals for PIs, dihedral angles between the two phenyl rings of benzophenone, and their HOMO–LUMO energy gaps

PIs	Geometry	θ/°	HOMO	LUMO	Gap/eV
BP-NB	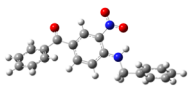	50.5	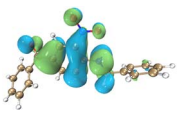	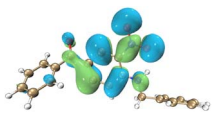	3.54
BP-NBtBu	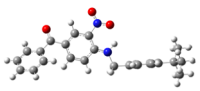	50.6	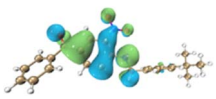	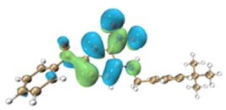	3.53
BP-NBI	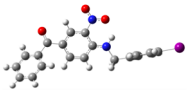	50.6	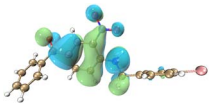	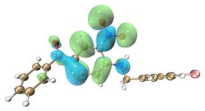	3.54
BP-$NBCF_3$	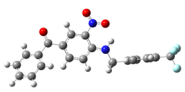	50.9	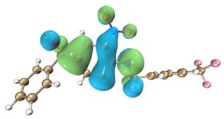	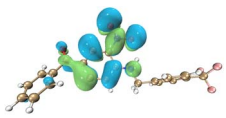	3.55

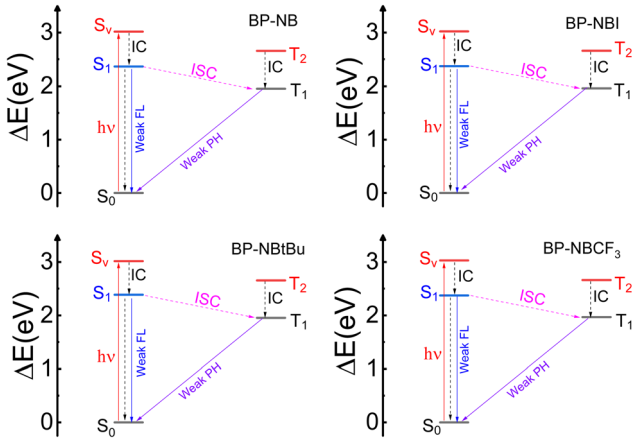

Fig. 2 Jabłoński-type diagram showing the singlet state and triplet state energies relative to that of the S_0 state for **BP-NBR**. (IC: internal conversion; ISC: intersystem crossing; FL: fluorescence; PH: phosphorescence).

promoted from S_0 to S_v. Subsequently, S_v underwent a rapid internal conversion (IC) to S_1. From S_1, several deactivation pathways were possible: return to the ground state (S_0) *via* IC, fluorescence emission, photochemical reaction, or intersystem crossing (ISC) to the higher triplet state T_2. The T_2 state then decayed internally to the lowest triplet state T_1, which could further undergo photochemical reactions.

To accurately elucidate the nature of electron excitations and explore the degree of intramolecular charge distribution in the **BP-NBR** systems, we employed the hole–electron analysis method. The distribution of holes and electrons in the singlet excited state is presented in Table 2. In the diagrams, the orange and blue denote electron and hole densities, respectively, with electron exciton occuring from the blue regions (holes) to the orange regions (electrons). In the S_1 state, electrons are predominantly concentrated on the nitro group, while holes are mainly located on the $-NCH_2-$ and CO groups, indicating an electronic transition from the $-NCH_2-$ and CO groups to the nitro group.

2.3 Photopolymerization kinetics

To evaluate the efficiency of these compounds as PIs, photopolymerization kinetics studies were performed upon irradiation with 405 nm LED light. Results indicated that **BP-NBR** were able to initiate the free radical polymerization of HDDA,

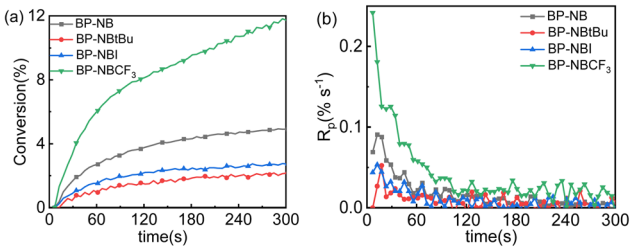

Fig. 3 Photopolymerization profiles of HDDA initiated by PIs upon exposure to 405 nm LED light (I = 120 mW cm^{-2}): (a) double bond conversion *vs.* time and (b) R_p *vs.* time; [PI] = 1%.

indicating their lower reactivity compared with 4-bis(benzylamino) benzophenone derivatives.[50] The final conversion achieved with **BP-NBR** was 2–12%. The photoinitiated rates (R_p) followed the order of BP-$NBCF_3$ > BP-NB > BP-NBI > BP-NBtBu. As shown in Table 1, the dihedral angles between the two phenyl rings of the benzophenone segment range from 50.5°–50.9° for **BP-NBR**, confirming their non-coplanar geometry. This twisted conformation provided a structural rationale for the low initiating activity in one-component **BP-NBR** systems (Fig. 3). In conventional benzophenone-based type II PIs, a coplanar conformation facilitates intersystem crossing to the reactive triplet state and subsequent hydrogen abstraction. The pronounced non-planarity observed here ($\theta \approx 50°$) likely disrupted this process, rendering the benzophenone moiety photochemically inactive. The 2-benzylamio-nitrophenyl segment, which maintained a push–pull configuration, served as the actual photosensitizing unit. Additionally, in the **BP-NBR** structure, the nitrobenzene segments abstract hydrogen from the benzyl amino group due to the formation of an intramolecular hydrogen bond between the nitro and benzyl amino groups. Then nitrogen-centered radicals may be yielded, but their instability makes them inefficient at adding to acrylate monomers, resulting in low initiation activity of the one-component initiating system.

However, **BP-NBR** were efficiently activated in the presence of ethyl 4-(dimethylamino)benzoate (EDB). Under various LEDs exposures, **BP-NBR**/EDB successfully initiated the polymerization of HDDA, and the photopolymerization kinetics profiles are shown in Fig. 4. The final conversion achieved with different **BP-NBR**/EDB systems was nearly identical. The photoinitiated rates followed the order of BP-$NBCF_3$ > BP-NBI ≥ BP-NB > BP-NBtBu. This can be attributed to the physical constraints inherent in

Table 2 Distribution of the holes and electrons of **BP-NBR** in the singlet excited state

PIs	BP-NB	BP-NBI	BP-NBtBu	BP-$NBCF_3$
$S_0 \rightarrow S_1$	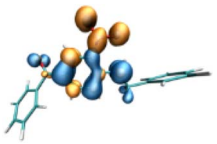	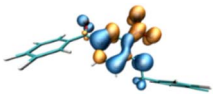	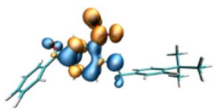	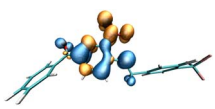

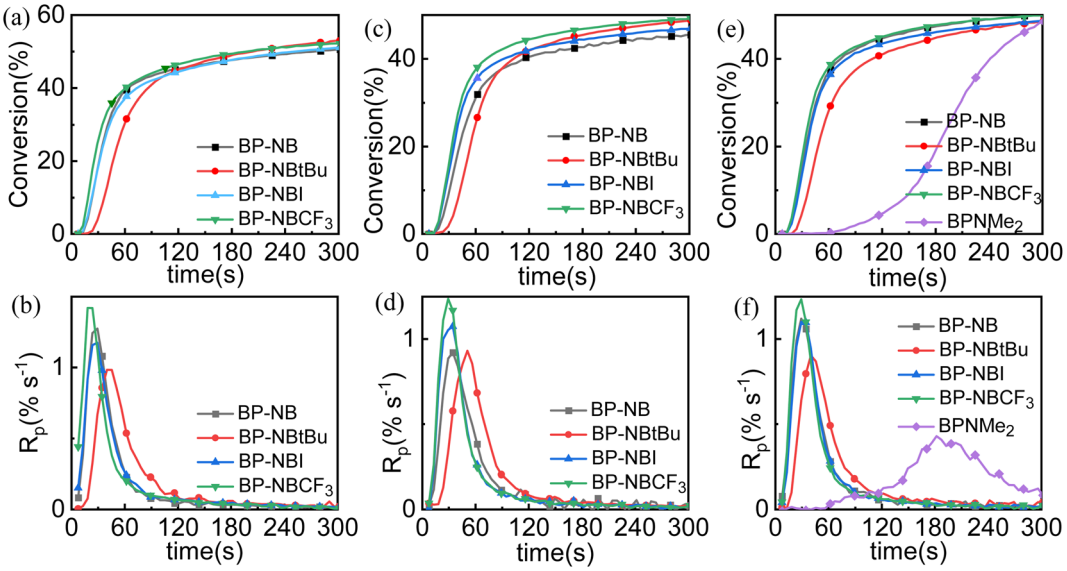

Fig. 4 Photopolymerization profiles of HDDA initiated by PIs/EDB upon exposure to different LEDs: (a and b): 405 nm, (I = 120 mW cm^{-2}); (c and d): 435 nm (I = 110 mW cm^{-2}); and (e and f): 450 nm (I = 140 mW cm^{-2}). (a, c and e): double bond conversion *vs.* time and (b, d and f): R_p *vs.* time; [PI] = 1%, [EDB] = 3%.

the photopolymerization reaction. The termination of the polymerization reaction was primarily governed by the limitation of chain segment mobility resulting from the glass transition of the system. As the reaction approached high conversion, the system viscosity increased dramatically, hindering the diffusion of the remaining double bonds and thereby terminating the polymerization. Consequently, although the initiation rate determined the time required to reach the gel point, all systems achieved a similar ultimate conversion dictated by the glass transition of the system.

For comparison, $BPNMe_2$ was employed as a benchmark PI and was irradiated with 450 nm LED light (Fig. 4e and S19). The **BP-NBR**/EDB systems showed a higher initiation rate and final conversion than the $BPNMe_2$/EDB, BP/EDB and ITX systems. The final conversion of **BP-NBR**/EDB was lower than that of the TPO system or ITX/EDB systems. In these systems, the nitrobenzene moiety, in combination with tertiary amines, has been reported to act as an efficient PI for acrylic monomers.[37] As shown in Fig. 5a and b, when **BP-NBR** were used at the same molar ratio relative to the monomer, the photoinitiation rate followed the order of BP-$NBCF_3$ > BP-NBI > BP-NB > BP-NBtBu. Furthermore, **BP-NBR** were capable of initiating the polymerization of HDDA in the presence of Iod. The corresponding photopolymerization profiles are presented in Fig. 5c and d. In this case, the order of photoinitiation rate was BP-NB > BP-NBtBu ≈ BP-NBI > BP-$NBCF_3$.

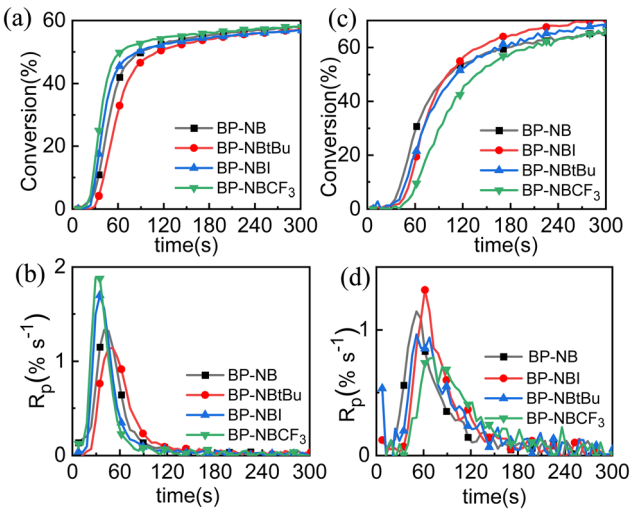

Fig. 5 Photopolymerization profiles of HDDA initiated by (a and b) PIs/EDB and (c and d) PIs/Iod upon 405 nm LED light irradiation (I = 120 mW cm^{-2}). (a and c): double bond conversion *vs.* time and (b and d): R_p *vs.* time; [PI] = 2 × 10^{-5} mol g^{-1}, [EDB] = [Iod] = 5 × 10^{-5} mol g^{-1}.

2.4 Photochemical mechanism

The photolysis behavior of BP-NB in various systems was investigated, with the corresponding spectral changes shown in Fig. 6. Upon irradiation with 405 nm LED light, the absorption spectrum of BP-NB alone initially decreased within the first 5 minutes, followed by an increase upon prolonged exposure. A similar trend was observed in the presence of EDB: the absorbance decreased after 5 min of irradiation and then increased with continued illumination. In contrast, the steady-state photolysis of BP-NB in the presence of Iod proceeded slowly under the same irradiation conditions, with the absorbance decreasing monotonically over time and no subsequent increase. This distinct behavior was directly associated with the specific interaction between BP-NB and Iod.

Electron paramagnetic resonance spin trapping (EPR-ST) experiments were carried out at room temperature to identify the active radicals generated in different BP-NB-based systems using *α*-phenyl-*N*-*tert*-butylnitrone (PBN) as the trapping agent.

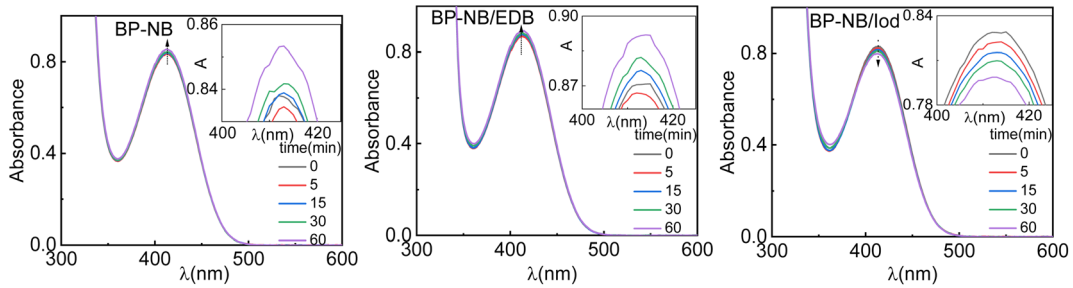

Fig. 6 Photolysis spectra of BP-NB in different systems upon 405 nm LED light irradiation for different times. ([BP-NB] = 1.5 × 10^{-4} mol L^{-1}, [EDB] = [Iod] = 3 × 10^{-3} mol L^{-1} in acetonitrile).

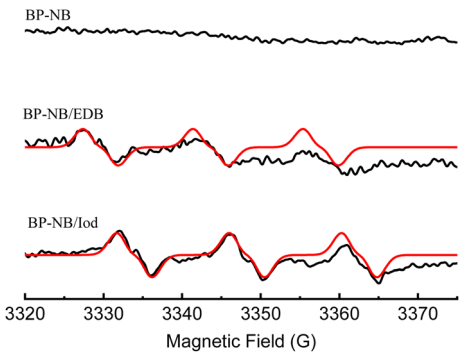

Fig. 7 EPR-ST spectra of the radical adduct captured by PBN in different photoinitiating systems in tert-butylbenzene exposed to 405 nm LED light (black line: experimental spectra; red line: simulated spectra).

As shown in Fig. 7, no active radicals were detected in the system containing BP-NB in tert-butylbenzene alone.[51] In contrast, in the presence of EDB, the aminoalkyl radicals were observed in the BP-NB/EDB system, with hyperfine coupling constants of α_N = 14.0 G and α_H = 2.3 G. For the BP-NB/Iod system, the detected radical exhibited hyperfine coupling constants of α_N = 14.3 G and α_H = 2.3 G.

The proposed photochemical mechanism of **BP-NBR** is illustrated in Scheme 3. **BP-NBR** are bifunctional molecules containing both electron donor and acceptor groups.[52] Upon irradiation, **BP-NBR** absorb photons and get promoted to an excited state. Then, a photochemical hydrogen atom transfer occurs from the amine to the nitro segment, facilitated by the formation of a hydrogen-bonded complex during the reaction.[53,54] This process may involve both intramolecular and intermolecular hydrogen transfers. Given that hydrogen bonds are present in the ground state of **BP-NBR**, the intramolecular pathway is likely predominant. The photoinduced intramolecular hydrogen transfer disrupts the extended conjugated system of the excited-state **BP-NBR**, leading to a decrease in absorbance. Subsequently, a nitrogen-centered radical is generated. The nitrogen radical is unstable and reacts poorly with monomers. Further, it cannot be captured by PBN. Consequently, no radical species were detected by EPR-ST in the BP-NB system, which aligned well with the photopolymerization results. The final products resulting from radical quenching possessed a larger and more stable conjugated system, exhibiting enhanced absorption near the λ_{max} (or at longer wavelengths). This is corroborated by the photolysis results, which showed enhanced absorption at longer wavelengths after exposure times exceeding 15 min.

The proposed mechanism for **BP-NBR** in the presence of EDB is shown in Scheme 4. Although **BP-NBR** alone exhibits certain stability, it has been found to undergo intermolecular

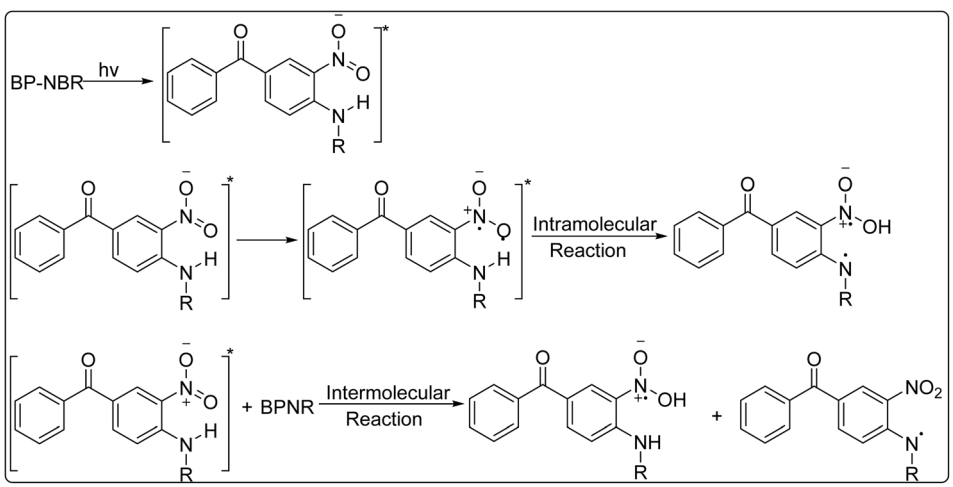

Scheme 3 Proposed mechanism for the one-component **BP-NBR** systems.

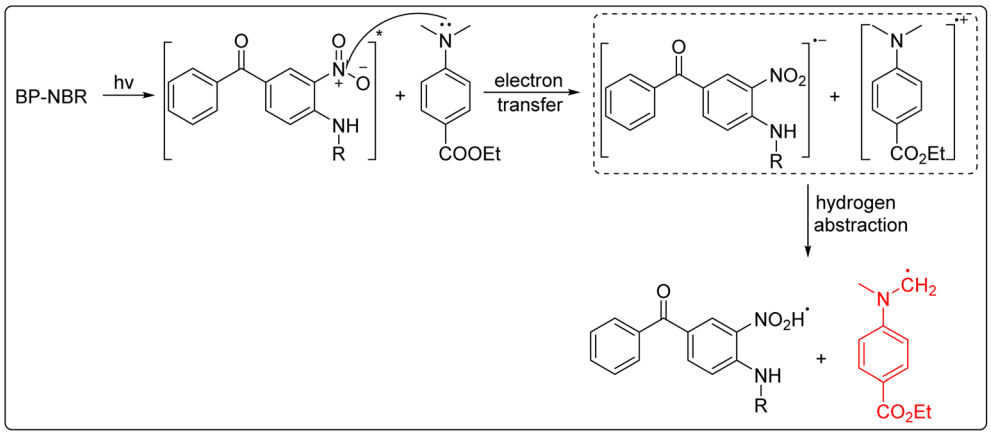

Scheme 4 Proposed mechanism of the **BP-NBR**/EDB system.

hydrogen abstraction in the presence of EDB.[55] The interaction between **BP-NBR** and EDB involves an electron transfer reaction, followed by proton transfer, generating the EDB-derived radical ($EDB^{\cdot}_{(-H)}$) capable of initiating free radical polymerization.[56,57] This proposed pathway was consistent with both the EPR-ST and photopolymerization results. Additionally, the absorbance of BP-NB in the BP-NB/EDB system was slightly higher than that in the one-component **BP-NBR** systems, suggesting that **BP-NBR** and EDB formed a weak charge transfer complex in the ground state.

The proposed mechanism for **BP-NBR** in the presence of Iod is shown in Scheme 5. Upon irradiation, **BP-NBR** absorb a photon and get promoted to an excited state (either singlet or triplet). Subsequently, an electron transfer occurs from the excited **BP-NBR** (donor) to Iod (acceptor). This interaction ultimately leads to the generation of an aryl radical (Ar·), which serves as the initiating species for free radical polymerization. The formation of Ar· was confirmed by the EPR-ST results. Specifically, the phenyl radicals (Ar·) were detected as PBN/Ar· radical adducts upon the irradiation of the BP-NB/Iod solution; simulation of the experimental EPR spectrum yielded hyperfine coupling constants of $\alpha_N = 14.3$ G and $\alpha_H = 2.3$ G. These radicals were 4-*tert*-butylphenyl radicals derived from Iod, and the results were consistent with the previous studies.[58–61] Based on the EPR-ST investigation and real-time FTIR experiments, aryl radicals were generated in this bimolecular photoinitiating system upon visible LED irradiation. In the **BP-NBR**/Iod photolysis system, the absorbance of **BP-NBR** decreased rapidly upon irradiation, with no subsequent increase observed in contrast to the behavior seen in the **BP-NBR** alone or **BP-NBR**/EDB systems (Fig. 6).

The Rehm–Weller equation was employed to calculate the free energy change associated with the photoinduced electron transfer from the donor to acceptor. To perform these calculations, the photoredox properties of all the components of the photoinitiating system were required. Therefore, the reduction and oxidation potentials of **BP-NBR** were determined by cyclic voltammetry (Fig. 8). The free energy changes (ΔG_{et}) for the electron transfer processes were then calculated using the classical Rehm–Weller equation, and the results are shown in Table 3. As shown, the $\Delta G_{et}{}^{S1}$ values were all negative, indicating that both the electron transfers from **BP-NBR** to Iod and EDB to **BP-NBR** were thermodynamically favorable.[62]

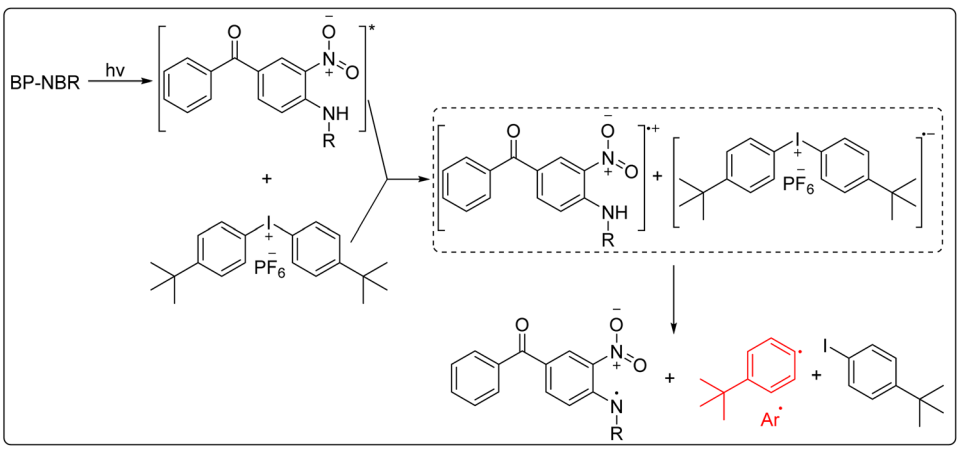

Scheme 5 Proposed mechanism for the **BP-NBR**/Iod system.

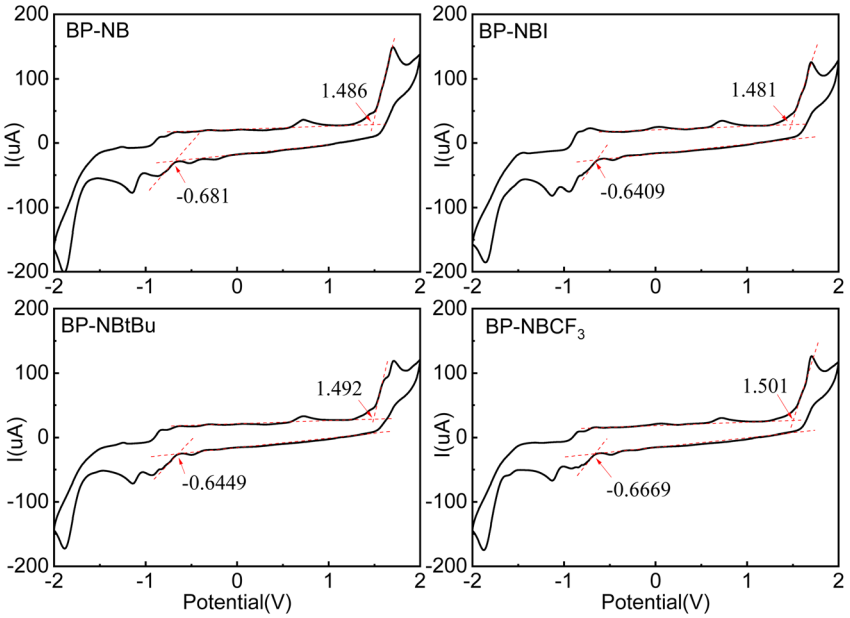

Fig. 8 Cyclic voltammograms for **BP-NBR** in acetonitrile.

Table 3 Parameters for characterizing the free energy changes of the PET reaction between PIs and Iod or EDB[a]

PIs	E_{ox} (V)	E_{red} (V)	E_{s1}	ΔG_{et}^{s1} (eV)	ΔG_{Iod}^{s1} (eV)	ΔG_{EDB}^{s1} (eV)
BP-NB	1.49	−0.68	2.36	−0.19	−0.19	−0.68
BP-NBI	1.48	−0.64	2.37	−0.25	−0.21	−0.73
BP-NBtBu	1.49	−0.64	2.39	−0.26	−0.22	−0.75
BP-NBCF$_3$	1.50	−0.67	2.37	−0.20	−0.19	−0.70

[a] E_{S1}-siglet state energy calculated from molecular orbital calculations. The reduction potential for the diaryliodonium salt: E_{red}Iod = −0.68 V *vs.* SCE;[63,64] the oxidation potential for the EDB: E_{ox}EDB = 1.00 V *vs.* SCE.[65,66]

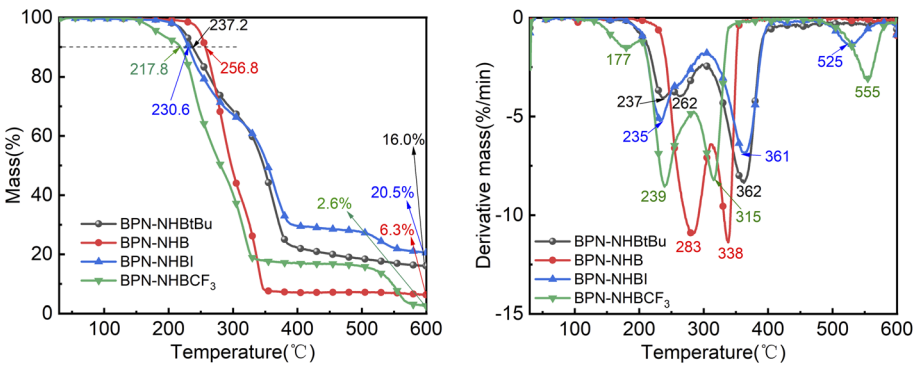

Fig. 9 TGA and DTG thermograms of **BP-NBR** under a nitrogen atmosphere.

2.5 Thermal stability

Thermogravimetric analysis (TGA) was performed to evaluate the thermal stability of **BP-NBR**. The corresponding thermogravimetric analysis/differential thermogravimetric(TGA/DTG) thermograms are presented in Fig. 9. Under an N_2 atmosphere, the temperatures corresponding to 10 wt% weight loss (T_d) ranged from 218 °C to 256 °C, following the order of BP-NB (256.8 °C) > BP-NBtBu (237.2 °C) > BP-NBI (230.6 °C) > BP-NBCF$_3$ (217.8 °C). The onset of decomposition varied among the derivatives: BP-NBCF$_3$ began to decompose at around 150 °C, BP-NBtBu and BP-NBI at around 200 °C, and BP-NB at around 230 °C, followed by a rapid weight loss in all cases. The residual char yields at elevated temperatures followed the order of BP-NBI (20.5%) > BP-NBtBu (16.0%) > BP-NB (6.3%) > BP-NBCF$_3$ (2.6%). These results demonstrated that the electron-withdrawing CF_3 group significantly accelerated thermal

decomposition, while the electron-donating *tert*-butyl group imparted intermediate stability, and the unsubstituted BP-NB showed the highest thermal resistance at 150–250 °C. In the temperature range of 350–600 °C, **BP-NBR** underwent a continuous weight loss, without distinct multiple decomposition steps, suggesting a single-stage degradation mechanism for all variants. However, the variation in residual char yields implied differences in the degradation pathways: BP-NBI and BP-NBtBu appeared to undergo partial carbonization, while BP-NB and BP-NBCF$_3$ decomposed completely to volatile products. The electron-donating nature of the *tert*-butyl and heavy iodide groups stabilized intermediate radical species, promoting recombination and char formation, while the electron-withdrawing CF_3 group favored fragmentation and volatilization. The TGA experiment demonstrated that the **BP-NBR** possess excellent thermal stability and storage stability, meeting the requirements for industrial applications.[67]

3. Conclusions

In summary, four (4-benzylamino-3-nitrophenyl) (phenyl) methanone derivatives (**BP-NBR**) were synthesized and utilized in free radical photopolymerization. These compounds exhibited broad absorption in the 350–500 nm range, enabling efficient overlap with the emission spectra of commercially available LEDs. Although **BP-NBR** alone showed low initiating activity under LED irradiation, they effectively sensitized both Iod and EDB in two-component photoinitiating systems. Notably, the **BP-NBR**/EDB systems exhibited faster photoinitiation rates than the commercial benchmark BPNMe$_2$/EDB system under 450 nm LED light irradiation, demonstrating their superior performance at longer wavelengths. Mechanism studies indicated that the 2-benzylamino-nitropehnyl segment serves as the photosensitizing unit. The para-substituent on the benzylamino group significantly influenced the photoinitiation efficiency, with electron-withdrawing groups (CF_3) enhancing the initiation rate in the presence of EDB and electron-donating groups (*tert*-butyl) showing higher activity in combination with Iod. Thermogravimetric analysis confirmed their good thermal stability, meeting the requirements for industrial applications. The findings of this work highlight the potential of push–pull benzophenone derivatives as versatile photosensitizers for long-wavelength LED photopolymerization.

Conflicts of interest

The authors declare no competing financial interests.

Data availability

The data supporting this article have been included as part of the supplementary information (SI). Other experimental data are available from the corresponding author upon reasonable request. Supplementary information: the experimental part, detailed structural characterization data and the choice of computational methods. See DOI: https://doi.org/10.1039/d6ra01087c.

Acknowledgements

This work was supported by the Guizhou Provincial Major Scientific and Technological Program (QKHZDZXZ[2024]022), Guizhou Provincial Science and Technology Projects (ZD[2025]034), and Guizhou Provincial Key Laboratory of Critical Materials and Devices for Solid-State Batteries (No. ZSYS(2025)036).

Notes and references

1 S. Chatani, C. J. Kloxin and C. N. Bowman, The power of light in polymer science: photochemical processes to manipulate polymer formation, structure, and properties, *Polym. Chem.*, 2014, **5**, 2187–2201.
2 M. Jankowska, A. Chachaj-Brekiesz, K. Trembecka-Wójciga, A. Jarzębska, M. Topa-Skwarczyńska, M. Pilch and J. Ortyl, Novel multi-material photo-curable resins containing high-performance photoinitiating systems and nano additives dedicated to 3D-VAT printing, *Polym. Chem.*, 2023, **14**, 2088–2106.
3 E. Hola, M. Pilch and J. Ortyl, Thioxanthone derivatives as a new class of organic photocatalysts for photopolymerisation processes and the 3D printing of photocurable resins under visible light, *Catalysts*, 2020, **10**, 1–28.
4 P.-M. Martínez-Rubio, O. Platnieks, M.-D. Avilés, M. Jurinovs, R. Pamies, M. Veseta, F.-J. Carrion-Vilches and S. Gaidukovs, High-performance bio-based UV-curable coatings with tunable mechanical and tribological properties, *Prog. Org. Coat.*, 2026, **213**, 109949.
5 Q. Zhou, S. Chen, X. Guo, C. Zhou and M. Jin, New water-soluble coumarin-ketone-pyridium salts photoinitiators for antibacterial coatings under visible LED photocuring, *Eur. Polym. J.*, 2025, **230**, 113896.
6 L. Qian, H. Xu, Y. Lu and Z. Chen, Preparation and performance optimization of PVP/PVA coatings with high adhesion and high hydrophilicity for coronary guidewires, *Prog. Org. Coat.*, 2025, **209**, 109600.
7 T. Gao, Z. Liu, J. Yin, J. Feng, C. Dietlin, F. Morlet-Savary, M. Schmitt, T. Petithory, L. Pieuchot, J. Zhang, F. Dumur, J. Lalevée and P. Xiao, Novel low-cytotoxic and highly efficient Type I photoinitiators for visible LED-/sunlight-induced photopolymerization and high-precision 3D printing, *Angew. Chem., Int. Ed.*, 2025, **64**, e202425598.
8 V. M. Soares, A. C. Reis and M. L. C. Valente, The influence of 2,4,6-trimethylbenzoyldiphenyl phosphine oxide on the toxicity of dental resins: A systematic review of *in vitro* studies, *Int. J. Adhes. Adhes.*, 2025, **138**, 103922.
9 P. Wang, J. Li, J. Yang, G. Wang, L. He and H. Zhang, Enabling 3D multilayer electronics through the hybrid of vat photopolymerization and laser-activated selective metallization, *Addit. Manuf.*, 2023, **74**, 103717.
10 T. Schlotthauer, D. Nolan and P. Middendorf, Influence of short carbon and glass fibers on the curing behavior and accuracy of photopolymers used in stereolithography, *Addit. Manuf.*, 2021, **42**, 102005.

11 T. Tong and D. Mo, Tunable optoelectronic performances of aminated benzothiadiazole-based D-A-D conjugated electrochromic polymers, *Polymer*, 2024, **310**, 127478.
12 E. D. Arabacı, O. Karakurt, A. Cirpan, E. Yildirim and A. M. Onal, The impact of π-bridge moiety on the optoelectronic properties and photochemical stabilities of benzodithiophene-based conjugated polymers, *Polymer*, 2024, **313**, 127736.
13 Y. Yagci, S. Jockusch and N. J. Turro, Photoinitiated polymerization: advances, challenges, and opportunities, *Macromolecules*, 2010, **43**, 6245–6260.
14 K. Starzak, W. Tomal, A. Chachaj-Brekiesz, M. Galek and J. Ortyl, Revealing the photoredox potential of azulene derivatives as panchromatic photoinitiators in various light-initiated polymerization processes, *Polym. Chem.*, 2024, **15**(29), 2931–2948.
15 Q. Wu, H. Shen, Y. Yang, F. Li and M. Deng, Thioxanthone-chalcone derivatives for LED photopolymerization, *Prog. Org. Coat.*, 2026, **211**, 109827.
16 Q. Zhou, S. Chen, X. Fan, Y. Li, X. Guo, C. Zhou, C. Bao and M. Jin, A multifunctional LED sensitive photoinitiator enables antibacterial hydrogel fabrication with spatiotemporal precision, *ACS Appl. Polym. Mater.*, 2025, **7**(15), 9880–9890.
17 M. Tian, Y. Gao, J. Nie and F. Sun, Construction of near-infrared gradient hydrogel actuators using self-floating induction and LED photopolymerization, *J. Colloid Interf. Sci.*, 2025, **685**, 1143–1153.
18 X. Sun, M. Yi, X. He, J. Qu, S. Fan, B. Xiang, B. Yuan, P. Luo, T. Wang, Y. Zou and Y. Pang, Coumarin derivatives as amphiphilic photoinitiators for free radical and cationic photopolymerizations with UV-vis LED irradiation, *Eur. Polym. J.*, 2025, **226**, 113743.
19 M. Yuan, S. Zhu, R. Chen, M. Lan, C. Yang, C. Zhou, X. Wang, T. Xu and L. Wang, Novel A-D-A structured triphenylamine derivatives for visible-LED photoinduced free radical polymerization under air, *Dyes Pigments*, 2026, **245**, 113248.
20 S. Fan, X. Sun, H. Liu, X. Qi, J. Lou, P. Wang, Y. Pang, Y. Zou and J. Wei, Electronic substituent effects on ketocoumarin-based photoinitiators: Structure-activity relationships for high-efficiency LED photopolymerization, *Prog. Org. Coat.*, 2025, **204**, 109229.
21 C. Dietlin, S. Schweizer, P. Xiao, J. Zhang, F. Morlet-Savary, B. Graff, J. P. Fouassier and J. Lalevée, Photopolymerization upon LEDs: new photoinitiating systems and strategies, *Polym. Chem.*, 2015, **6**, 3895–3912.
22 F. Dumur, Recent advances on visible light triphenylamine-based photoinitiators of polymerization, *Eur. Polym. J.*, 2022, **166**, 111036.
23 F. Dumur, D. Gigmes, J. P. Fouassier and J. Lalevée, Organic electronics: an El Dorado in the request of new photocatalysts for polymerization reactions, *Acc. Chem. Res.*, 2016, **49**(9), 1980–1989.
24 P. Xiao, J. Zhang, F. Dumur, M. A. Tehfe, F. Morlet-Savary, B. Graff, D. Gigmes, J. P. Fouassier and J. Lalevée, Visible light sensitive photoinitiating systems: Recent progress in cationic and radical photopolymerization reactions under soft conditions, *Prog. Polym. Sci.*, 2015, **41**, 32.
25 J. Kabatc, J. Ortyl and K. Kostrzewska, New kinetic and mechanistic aspects of photosensitization of iodonium salts in photopolymerization of acrylates, *RSC Adv.*, 2017, **7**, 41619–41629.
26 S. Chen, W. D. Cook and F. Chen, Photopolymerization of vinyl ether networks using an iodonium initiator: Effect of radiation intensity and iodonium concentration, *Macromolecules*, 2009, **42**(16), 5965–5975.
27 X. Nan, Y. Huang, Q. Fan and J. Shao, Efficient visible photoinitiator containing linked dye-coinitiator and iodonium salt for free radical polymerization, *Prog. Org. Coat.*, 2015, **81**, 11–18.
28 J. A. Kampmeier and T. W. Nalli, Initiation of cationic polymerization of cyclic ethers by redox radical-chain reactions of onium salts, *J. Org. Chem.*, 1994, **59**(6), 1381–1388.
29 J. V. Crivello and J. J. W. Lam, Diaryliodonium salts. A new class of photoinitiators for cationic polymerization, Symmetric meta-terphenyl derivatives as visible light photosensitizers: Advancing iodonium salt-based 3D printing nanocomposites, *Macromolecules*, 1977, **10**(6), 1307–1315.
30 M. Jankowska, M. Klamut, I. Zaborniak, E. Hola, A. Gruchala-Halat, P. Szymaszek, K. Starzak, J. Pietraszewski, P. Bloniarz, A. Sobkowiak, M. Galek, P. Chmielarz and J. Ortyl, Symmetric meta-terphenyl derivatives as visible light photosensitizers: Advancing iodonium salt-based 3D printing nanocomposites, *Polymer*, 2026, **344**, 129468.
31 W. Tomal, M. Pilch, A. Chachaj-Brekiesz, M. Galek, F. Morlet-Savary, B. Graff, C. Dietlin, J. Lalevée and J. Ortyl, Photoinitiator-catalyst systems based onmeta-terphenyl derivatives as photosensitisers of iodonium and thianthrenium salts for visible photopolymerization in 3D printing processes, *Polym. Chem.*, 2020, **11**(28), 4604–4621.
32 W. Tomal, P. Szymaszek, M. Bilut, R. Popielarz, T. Świergosz and J. Ortyl, meta-Terphenyls as versatile fluorescent molecular sensors for monitoring the progress of hybrid polymerization processes, *Polym. Chem.*, 2022, **13**(32), 4650–4665.
33 E. Hola, M. Topa, A. Chachaj-Brekiesz, M. Pilch, P. Fiedor, M. Galek and J. Ortyl, New, highly versatile bimolecular photoinitiating systems for free-radical, cationic and thiol-ene photopolymerization processes under low light intensity UV and visible LEDs for 3D printing application, *RSC Adv.*, 2020, **10**(13), 7509–7522.
34 A. A. Mousawi, F. Dumur, P. Garra, J. Toufaily, T. Hamieh, B. Graff, D. Gigmes, J. P. Fouassier and J. Lalevée, Carbazole scaffold based photoinitiator/photoredox catalysis: Toward new high performance photoinitiating systems and application in LED projector 3D printing resins, *Macromoelcules*, 2017, **50**(7), 2747–2758.
35 H. Hayek, M. Guergueb, F. Mouhoubi, S. Lajnef, F. Peyrot, L. Michely, X. Chen, Y. Wu, J. Zhao, A. Dolbecq, O. Oms, P. Mialane and D.-L. Versace, Polyoxometalate-derived

porphyrins as promising visible light photo-initiating systems for antibacterial applications, *Eur. Polym. J.*, 2025, **240**(19), 114316.

36 A. Pietraszek, F. Petko and J. Ortyl, Recent advances in aminonitrile derivatives as components of visible light photoinitiating systems for photopolymerization processes in VPP 3D printing: photoinitiators in two- and multicomponent systems, *Eur. Polym. J.*, 2025, **237**, 114162.

37 S. Li, G. Ma and J. Qu, Novel benzophenone derivatives photoinitiators based on carbazole group for deep curing and fast 3D printing, *J. Photochem. Photobio. A*, 2025, **460**, 116144.

38 T. L. Huang, Y. H. Li and Y. C. Chen, Benzophenone derivatives as novel organosoluble visible light Type II photoinitiators for UV and LED photoinitiating systems, *J. Polym. Sci.*, 2020, **58**(20), 2914–2925.

39 W. Li, J. Nie, Y. Zhao and X. Zhu, A low mobility UV-LED benzophenone photoinitiator, *J. Photochem. Photobiol. A*, 2024, **455**, 115785.

40 T. Xue, Y. Li, X. Zhao, J. Nie and X. Zhu, A facile synthesized benzophenone Schiff-base ligand as efficient type II visible light photoinitiator, *Prog. Org. Coat.*, 2021, **157**, 106329.

41 G. Jiang, Q. Li, A. Lv, L. Liu, J. Gong, H. Ma, J. Wang and B. Tang, Modulation of the intramolecular hydrogen bonding and push-pull electron effects toward realizing highly efficient organic room temperature phosphorescence, *J. Mater. Chem. C*, 2022, **10**, 13797–13804.

42 R. Lopez-Arteaga, A. B. Stephansen, C. A. Guarin, T. I. Sølling and J. Peon, The influence of push-pull states on the ultrafast intersystem crossing in nitroaromatics, *J. Phys. Chem. B*, 2013, **117**, 9947–9955.

43 V. V. Volchov, M. N. Khimich, M. V. Rusalov, F. E. Gostev, I. V. Shelaev, V. A. Nadtochenko, S. P. Gromov and M. Y. Melnikov, Intramolecular photo-driven electron transfer in the series of DMABN related compounds with para-substituted acceptors. Study of the rate constants by Marcus theory, *J. Phys. Org. Chem.*, 2020, **33**(4), e4041.

44 A. K. Singh, G. Ramakrishna, H. N. Ghosh and D. K. Palit, Photophysics and ultrafast relaxation dynamics of the excited states of dimethylaminobenzophenone, *J. Phys. Chem. A*, 2004, **108**, 2583–2597.

45 A. Al Mousawi, F. Dumur, P. Garra, J. Toufaily, T. Hamieh, B. Graff, D. Gigmes, J. P. Fouassier and J. Lalevée, Carbazole scaffold based photoinitiator/photoredox catalysts: Toward new high performance photoinitiating systems and application in LED projector 3D printing resins, *Macromolecules*, 2017, **50**(7), 2747–2758.

46 N. M. O. Boyle, A. L. Tenderhol and K. M. Langer, cclib: A library for package-independent computational chemistry algorithms, *J. Comput. Chem.*, 2008, **29**, 839–845.

47 M. V. Encinas, A. M. Rufs, E. Norambuena and C. Giannotti, Polymerization of vinyl monomers photoinitiated by p-nitroaniline: photoinitiation mechanism, *J. Polym. Sci. Part A*, 2000, **38**, 2269–2273.

48 J. Wolleben and A. C. Testa, Charge transfer triplet state of p-nitroaniline, *J. Phys. Chem.*, 1977, **81**(5), 429–431.

49 W. Schuddeboom and J. M. Warman, Dipolar triplet states of p-nitroaniline and N-alkyl derivatives with one-, two-, and three-fold symmetry, *J. Phys. Chem.*, 1996, **100**, 12369–12373.

50 Q. Wu, H. Wang, Q. Zhang, F. Li and M. Deng, The synthesis and performance of benzophenone-based LED photoinitiators, *Paint Coat. Ind.*, 2024, **54**(4), 37–46.

51 S. K. Wong and J. K. S. Wan, Some electron spin resonance observations in the photoreduction of nitrobenzenes, *Can. J. Chem.*, 1973, **51**, 753–759.

52 A. N. Frolov, N. A. Kuznetsova and A. V. Eltsov, Intermolecular photochemical reduction of aromatic nitro-compounds, *Russ. Chem. Rev.*, 1976, **45**, 1024.

53 D. V. Ovsyannikov and S. V. Zelentsov, Role of complexation between monomethylamine and triplet nitromethane molecules in the hydrogen transfer reaction, *High Energ Chem*, 2019, **53**(2), 103–107.

54 P. L. Gkizis, I. Triandafillidi and C. G. Kokotos, Nitroarenes: the rediscovery of their photochemistry opens new avenues in organic synthesis, *Chem*, 2023, **9**, 3401–3414.

55 A. Costela, I. Carcia-Moreno, J. Dabrio and R. Sastre, Photophysics and photochemistry of p-nitroaniline as photoinitiator, *J. Photochem. Photobio. A*, 1997, **109**, 77–86.

56 M. V. Encinas, A. M. Rufs, E. Norambuena and C. Giannotti, Polymerization of vinyl monomers photoinitiated by p-nitroaniline: photoinitiation mechanism, *J. Polym. Sci. Part A*, 2000, **38**, 2269–2273.

57 V. F. Moreno, B. H. Barboza, L. M. Martins, C. Gaglieri, G. Bannach, A. Batagin-Neto and L. C. Silva-Filho, Novel quinoline photoinitiators for dimethacrylate monomer photopolymerization under UV and blue light, *Eur. Polym. J.*, 2024, **218**, 113331.

58 Q. Wu, H. Shen, M. Deng and C. Hao, Design, synthesis, and application of push-pull chalcone-based photoinitiators for free radical polymerization, *New J. Chem.*, 2025, **49**, 8653.

59 T. Borjigin, J. Feng, N. Giacoletto, M. Schmitt, F. Morlet-Savary, B. Graff, P. Xiao, M. Nechab, F. Gigmes, F. Dumur and J. Lalevée, Naphthoquinone-imidazolyl derivatives-based oxime esters as photoinitiators for blue LED-induced free radical photopolymerization, *Eur. Polym. J.*, 2024, **206**, 112801.

60 J. Lalevée, M. A. Tehfe, A. Zein-Fakih, B. Ball, S. Telitel, F. Morlet-Savary, B. Graff and J. P. Fouassier, N-Vinylcarbazole: An additive for free radical promoted cationic polymerization upon visible light, *ACS Macro Lett.*, 2012, **1**(7), 802–806.

61 J. Feng, T. Gao, F. Morlet-Savary, M. Schmitt, C. Dietlin, J. Zhang, X. Peng, P. Xiao, F. Dumur and J. Lalevée, Donor-π-acceptor photoinitiators for high-efficiency visible LED and sunlight polymerization and high-precision 3D printing, *Angew. Chem., Int. Ed.*, 2025, **64**(27), e202425198.

62 W. Tomal, K. Galuszka, P. Lepcio, M. Pilch, A. Chachaj-Brekiesz, M. Korcuskova and J. Ortyl, Naphthalene-stilbenes as effective visible-light sensitizers to study the effect of diluent and nanofillers on *in situ* photopolymerization and 3D-VAT printing process, *Mater. Adv.*, 2024, **5**, 2200242.

63 Q. Wu, J. Guo, K. Song, S. Xu, F. Li and M. Deng, Photoinitiation mechanism and ability of thioxanthone-based versatile visible photoinitiators, *Macro. Chem. Phys.*, 2022, **223**(23), 2200242.

64 M. Rahal, B. Graff, J. Toufaily, T. Hamieh, M. Ibrahim-Ouali, F. Dumur and J. Lalevée, Naphthyl-naphthalimides as high-performance visible light photoinitiators for 3D printing and photocomposites synthesis, *Catalysts*, 2021, **11**(11), 1269.

65 S. Liu, D. Brunel, G. Noirbent, A. Mau, H. Chen, F. Morlet-Savary, B. Graff, D. Gigmes, P. Xiao, F. Dumur and J. Lalevée, New multifunctional benzophenone-based photoinitiators with high migration stability and their applications in 3D printing, *Mater. Chem. Front.*, 2021, **5**, 1982.

66 T. Gao, F. Morlet-Savary, B. Graff, F. Dumur, J. Zhang, P. Xiao and J. Lalevée, Coumarin derivatives as dual photo/thermal initiators for free radical polymerization and 3D printing, *Polym. Chem.*, 2024, **15**, 2416–2427.

67 Q. Wu, H. Shen and M. Deng, High performance and low migration photoinitiators for LED photopolymerization: Thioxanthone-chalcone derivatives operating under visible light, *Polymer*, 2025, **339**, 129122.